IOPscience iopscience.iop.org

Home Search Collections Journals About Contact us My IOPscience

Spectroscopic properties of holmium doped $LiTaO_3$ crystals

This article has been downloaded from IOPscience. Please scroll down to see the full text article.

1998 J. Phys.: Condens. Matter 10 10291

(http://iopscience.iop.org/0953-8984/10/45/016)

View the table of contents for this issue, or go to the journal homepage for more

Download details:
IP Address: 171.66.16.210
The article was downloaded on 14/05/2010 at 17:51

Please note that terms and conditions apply.

J. Phys.: Condens. Matter **10** (1998) 10291–10306. Printed in the UK PII: S0953-8984(98)95952-5

Spectroscopic properties of holmium doped $LiTaO_3$ crystals

G Dominiak-Dzik†, S Gołab†, J Zawadzka†, W Ryba-Romanowski†,
T Łukasiewicz‡ and M Świrkowicz‡

† Institute of Low Temperature and Structure Research, Polish Academy of Sciences, 2 Okólna Street, 50-950 Wrocław, Poland

‡ Institute of Electronic Materials Technology, 133 Wólczyńska Street, 01-919 Warsaw, Poland

Received 16 July 1998

Abstract. The spectroscopic properties of Ho^{3+} ions in $LiTaO_3$ crystals have been investigated using optical absorption, luminescence and lifetime measurements in the 5–300 K temperature range. The low temperature, polarized absorption spectra of Ho^{3+} in this matrix have allowed us to identify the Stark levels of the different multiplets up to 30 000 cm^{-1}. The results are consistent with C_3 symmetry for the rare-earth ions and a singlet A character for the lowest Stark level of the $^5I_8$ ground state. Several transitions show additional structure which indicates multi-site occupancy for the Ho^{3+} ions. The measured oscillator strengths of the transitions between the J manifolds at 300 K are compared with those derived from the Judd–Ofelt theory. The radiative transition rates and radiative lifetimes have been calculated. The luminescence observed at 5 K has been attributed to $^5S_2 \rightarrow {}^5I_8$ (18 100 cm^{-1}), $^5F_5 \rightarrow {}^5I_8$ (15 060 cm^{-1}) and $^5S_2 \rightarrow {}^5I_7$ (13 150 cm^{-1}) transitions. The obtained data are used to discuss the radiative properties for luminescent levels of Ho^{3+} ions in the $LaTaO_3$ matrix. The emission cross-section of a potential laser line at 2 μm connected with the $^5I_7 \rightarrow {}^5I_8$ transition is estimated.

1. Introduction

Lithium niobate, $LiNbO_3$, is a well known ferroelectric material that has many applications to the technology of piezoelectric, optical and electrical–optical materials and devices. Lithium tantalate, $LiTaO_3$, is an isostructural material that has similar physical properties. The interest in $LiNbO_3$ and $LiTaO_3$ crystals doped with transition metal and rare earth ions has been renewed recently because of their potential application as self-Q switching and self-frequency-doubling laser materials. Attention has been focused on the $LiNbO_3$ crystal since its d_{31} nonlinear coefficient involved in second-harmonic generation (SHG) is considerably higher than that of $LiTaO_3$. Therefore, the literature concerning optical properties of doped $LiTaO_3$ crystals is not exhaustive and deals with Nd^{3+} [1–5], Yb^{3+} [6], Pr^{3+} [7], Tb^{3+} [8] and Cr^{3+} [9, 10] as dopants. The capability for efficient SHG by the quasi-phase-matched method, and a higher threshold for photorefractive damage in comparison to $LiNbO_3$ make doped $LiTaO_3$ crystals a potential self-frequency-doubling laser material.

2. Experimental details

Single crystals of $LiTaO_3$:Ho^{3+} were grown from a congruent melt (Li/Ta = 0.94) by the Czochralski method. Ho_2O_3 in a concentration of 0.5 at.% (9.5×10^{19} ions cm^{-3}) relative to Ta^{5+}, was added to the melt as a dopant. Examination of samples with an x-ray microprobe indicated that the actual concentration of Ho^{3+} ions is essentially the same as the nominal

0953-8984/98/4510291+16$19.50 © 1998 IOP Publishing Ltd

one. The crystals were oriented along the crystallographic *c* axis and next were cut to obtain samples with their faces parallel or perpendicular to the ferroelectric *c* axis.

Absorption spectra were measured with a Varian model 2300 spectrophotometer at 300 and 5 K. The spectral resolution was 0.2 nm in the UV–VIS and 0.8 nm in the IR region. Low temperature (5 K) luminescence was excited by a 460 nm line of an argon ion laser. The spectra were analysed with a Zeiss model GDM 1000 grating monochromator (with a bandwidth of 2 cm^{-1}) detected by a cooled photomultiplier and the resulting signal was averaged by an SRS 250 boxcar integrator. In luminescence decay time measurements a nitrogen laser pumped tunable dye laser was used as excitation source. For low temperature measurements the sample was placed in an Oxford model CF 1204 continuous flow helium cryostat equipped with a temperature controller.

3. Results and discussion

For clarity, this section of the paper is divided into two parts.

(i) *Absorption studies*—unpolarized and polarized absorption spectra from the ground multiplet $^5I_8$ of Ho^{3+} ions to excited states measured in the visible and near infrared region at 300 and 5 K. The experimental data allowed us to analyse the $4f^{10}$ electronic structure (character of transitions, their locations and assignments) of Ho^{3+} ions. Also we have obtained information about the multi-site structure for Ho^{3+} ions in the $LiTaO_3$ host. In this part we dealt with the intensity analysis of the absorption bands from Judd–Ofelt theory, which was used to predict various spectroscopic parameters such as radiative transition probabilities (A_r), radiative lifetimes (τ_r), branching ratios (β) and integrated absorption cross-section (σ_a) for the fluorescent levels of Ho^{3+} ions.

(ii) *Luminescence studies*—fluorescence measurements have been carried out in the visible and near infrared spectral region at 5 K. The emission data were used to determine the main fluorescent channels of Ho^{3+} ions in the $LiTaO_3$ matrix as well as to identify the Stark components of the $^5I_8$ ground level. Spectral data were used to estimate the emission cross-section of a potential laser line at 2 μm connected with the $^5I_7 \rightarrow {}^5I_8$ transition.

3.1. Absorption data

Because $LiTaO_3$ is a uniaxial crystal, anisotropic effects should be considered and thus polarized absorption spectra have been measured. Low temperature (5 K) polarized absorption spectra of Ho^{3+} ions in $LiTaO_3$ crystals are shown in figures 1 and 2. The samples were cut with their faces parallel to the crystallographic *c* axis. The π and σ spectra have been recorded with light polarized parallel (for π) and perpendicular (for σ) to the ferroelectric *c* axis. We have also measured α spectra which were taken from the sample with the *c* axis perpendicular to the face so the electric field of the unpolarized light was perpendicular to this axis. It is worth noting that the σ and α absorption spectra were very similar with regards to the character of the bands and the maxima positions.

The observed absorption lines are not fully resolved and all are strongly inhomogeneously broadened. We did not observe the absorption band associated with the transition from the $^5I_8$ ground state to the $^5I_4$ excited state located at about 13 300 cm^{-1} (750 nm) as the oscillator strength of this transition is very low.

Unfortunately, the electronic structure ($4f^{10}$) of Ho^{3+} ions is such that the visible and near infrared transitions involve levels having a high multiplicity $(2J+1)$ which gives a high number of Stark levels. This leads to strong level overlapping and consequently we observe

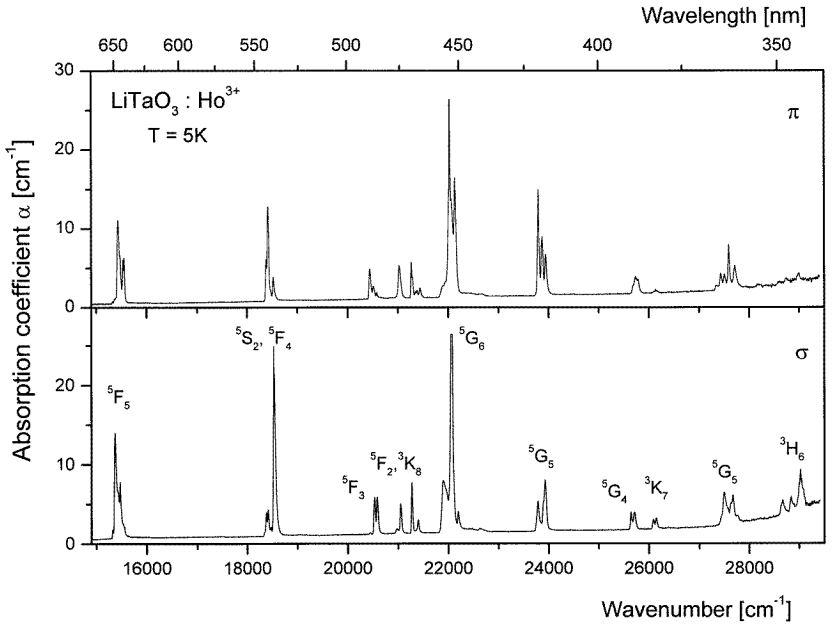

Figure 1. Polarized absorption spectra of Ho^{3+} ions in an $LiTaO_3$ crystal recorded in the 670–340 nm spectral range at 5 K.

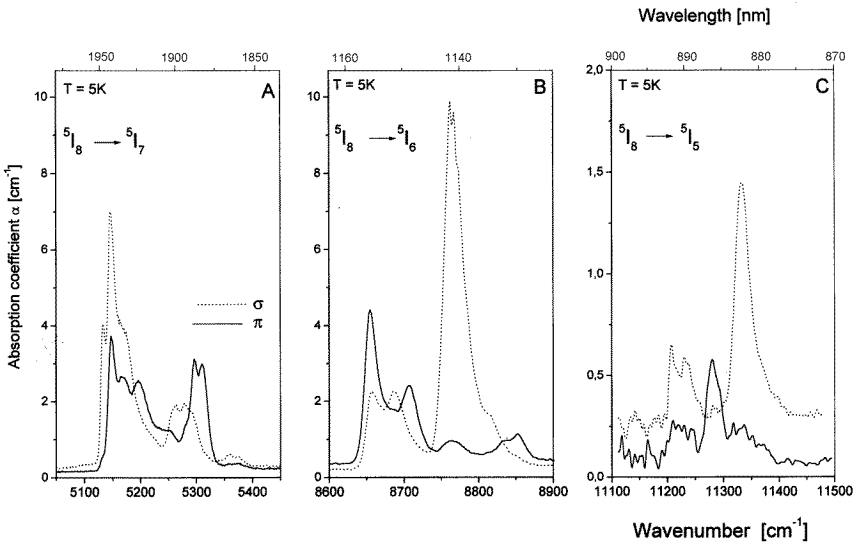

Figure 2. Absorption spectra of Ho^{3+} ions in an $LiTaO_3$ crystal recorded in the near infrared spectral range with light polarized perpendicular (dashed line) and parallel (solid line) to the optical axis of the crystal. $T = 5$ K.

a large number of absorption bands. Additionally, the presence of a large number of defects due to nonstoichiometry of the $LiTaO_3$ crystal could not be avoided in our consideration. The lattice location of trivalent ion (transition metal, rare earth) dopants in $LiXO_3$ (X = Nb,

Ta) crystals was studied by various techniques [11–13]. Cationic impurities enter the lattice by substituting for Li^+ and/or Ta^{5+} ions or in interstitial positions (free octahedron site and free tetrahedral site). The point symmetry of the impurity is C_3. According to group theory for C_3 symmetry any J levels of the Ho^{3+} ion in an $LiTaO_3$ host will split into a number of A and E Stark levels depending on the J value [14]. The electric-dipole selection rules and the number of crystal-field states for C_3 symmetry are presented in tables 1 and 2 respectively. One can see that the transitions between two A levels should be observed in π polarized spectra whereas the transitions between an E level and an A level are allowed in σ polarized systems.

Table 1. Electric-dipole selection rules for C_3 symmetry.

	A	E
A	π	σ, α
E	σ, α	π, σ, α

Table 2. Number of crystal-field states for C_3 symmetry.

	Number of Stark levels	
J value	A	E
2	1	2
3	3	2
4	3	3
5	3	4
6	5	4
7	5	5
8	5	6

In order to determine the energy and Stark components of Ho^{3+} levels in the $LiTaO_3$ crystal the low temperature polarized absorption spectra have been used. Most of the bands observed in the π polarized spectra disappear or drastically decrease their intensity in the σ polarized spectra although for some transitions contributions in σ and π spectra have been observed simultaneously. Minor contributions to the σ and π spectra at wavelengths coincident with the dominant peaks in the opposite polarization can be attributed to strong level overlapping.

Using the selection rules for the experimental data analysis we could infer that the lowest Stark component of the $^5I_8$ ground state is A (singlet) in character. The Stark level structure of the ground state has been established from a low temperature (5 K) unpolarized emission spectrum connected with the $^5S_2 \rightarrow {}^5I_8$ and $^5F_5 \rightarrow {}^5I_8$ transitions.

Despite the fact that the number of the experimentally observed lines is greater than predicted by the group theory, for some transitions it was not possible to resolve and to determine all Stark components. This is the case for the $^5I_8 \rightarrow {}^5I_7$ absorption spectrum presented in figure 2(A). Crystal-field theory predicts 10 lines (5A + 5E) for this transition. However, 11 lines have been experimentally detected in polarized spectra measured at 5 K. Only eight lines have been assigned as the Stark components of the $^5I_7$ level. Three lines are clearly split into doublets with energy difference about 16 cm^{-1} and with very similar

intensities. These pairs of lines have been identified as site splitting of the Stark levels due to non-identical sites existing in the $LiTaO_3$ crystal. This is evidence that in spite of a large number of lines not all the crystal-field levels of the $^5I_7$ state have been detected.

The assignment of Ho^{3+} levels in $LiTaO_3$, their energy and their symmetry character are gathered in table 3. The assignments are in good agreement with those for Ho^{3+} in $LiNbO_3$ crystals [15–17].

The observed structure of the $^5I_8$ ground state and of the excited levels of Ho^{3+} ions in the $LiTaO_3$ host is, generally, in accordance with the predicted multiplicity in C_3 symmetry. It is important to note that the fundamental and the first excited Stark level are not well separated, showing an energy difference $\Delta E = 10$ cm^{-1} only, a value comparable to that observed in the $LiNbO_3$ host. This is too small to ensure negligible population of the excited level even at 5 K. This induces overlapping between the levels and means that even at low temperature the observed absorption bands involve not only transitions originating from a fundamental level but also the transitions from the first excited Stark component. This means that the spectra are not simple in their structure.

3.1.1. Multi-site structure. For all the bands, examined in this work, the number of detected lines is greater than the group theory predicts for C_3 symmetry. The structure of low temperature optical bands gives evidence for the presence of at least three different Ho^{3+} sites in the $LiTaO_3$ crystal. As mentioned earlier $LiTaO_3$ crystals like $LiNbO_3$ ones provide a few different centres for co-doping ions. Different centres could be expected for ions entering different lattice sites (Ta^{5+} and/or Li^+) or for ions replacing the same lattice site (e.g. Li^+) but with a non-identical local environment. All of these sites, called 'nonequivalent centres', create the multi-site structure of the observed bands.

For Ho^{3+} ions in the $LiTaO_3$ host the multi-site structure is rich and brightly marked although most of the lines do not split in the crystal field. It is worth noting that many peaks detected in both σ and π spectra create pairs of unresolved lines with the energy difference about 5 cm^{-1}. Presented in figure 2(B) the σ polarized absorption band due to $^5I_8 \rightarrow {}^5I_6$ transition has a maximum that is very well split into two peaks: one at 8762 cm^{-1} and the second at 8767 cm^{-1}. These peaks are a good illustration for the existence of pairs of lines due to a nonidentical local crystal field. This small splitting ($\Delta E = 5$ cm^{-1}) cannot be explained in terms of a thermalization effect because the first excited Stark component of the $^5I_8$ level is 10 cm^{-1} above the ground state.

For some multiplets, an additional peak splitting of about 16 cm^{-1} (see figure 2(A)) have been detected suggesting again a multi-site occupancy of Ho^{3+} ions in the $LiTaO_3$ lattice. The clearest example of the existence of additional splitting within the absorption bands is the $^5I_8 \rightarrow {}^5S_2$ transition presented in figure 3. Although the $^5S_2$ and $^5F_4$ multiplets are close in energy, a low temperature study can safely separate them. The $^5S_2$ level has the lowest degeneracy ($J = 2$) of the observed multiplets and therefore the symmetry assignment is easier than for the remaining levels. In consequence, the appearance of the additional lines could correspond to different lattice sites. According to the C_3 symmetry selection rules one expects two σ and one π polarized lines. The low temperature absorption spectra show two weak bands with a σ symmetry (maxima at 18 330 cm^{-1} and 18 470 cm^{-1}) and two strong bands with a clear π character and with the energy difference of about $\Delta E = 34$ cm^{-1}. Within the most intense band in the π polarized spectrum a supplementary structure has been detected confirming the existence of a different local crystal field. Although this band does not split in the crystal field one can resolve it into at least four components with the maxima at 18 410, 18 415, 18 421 and 18 427 cm^{-1}.

Table 3. Energy levels and symmetry character of the Ho^{3+} multiplets in $LiTaO_3$ crystals.

$^{2S+1}L_J$	Wavelength λ (nm)	Wavenumber E (cm^{-1})	Symmetry character
$^5I_8$		0	A
		10	
		57	
		77	
		98	
		140	
		170	
		238	
		260	
		308	
		390	
$^5I_7$	1948.2	5 132	E
	1943.6	5 146	E
	1935.0	5 168	A
	1924.6	5 196	A
	1904.4	5 251	A
	1900.1	5 263	E (I)
	1894.3	5 279	E (II)
	1887.9	5 297	A (I)
	1882.9	5 311	A (II)
	1866.4	5 358	E (I)
	1860.8	5 374	E (II)
$^5I_6$	1155.4	8 655	A
	1151.2	8 687	E
	1148.5	8 707	A
	1147.5	8 715	A
	1141.3	8 762	E (I)
	1140.6	8 767	E (II)
	1134.7	8 813	E
	1132.0	8 834	A (I)
	1129.7	8 852	A (II)
$^5I_5$	892.3	11 207	E (I)
	891.5	11 217	E (II)
	890.6	11 229	E (I)
	889.8	11 238	E (II)
	888.5	11 255	E (I)
	888.1	11 260	E (II)
	886.5	11 280	A
	883.6	11 317	A
	882.5	11 332	E
$^5F_5$	652.6	15 323	E
	650.5	15 373	E
	647.9	15 435	A
	646.3	15 473	E
	645.2	15 500	E
	643.8	15 533	A (I)
	642.9	15 554	A (II)
$^5S_2$	545.6	18 330	E
	544.0	18 383	A*
	542.9	18 417	A* (I)

Table 3. Continued.

$^{2S+1}L_J$	Wavelength λ (nm)	Wavenumber E (cm^{-1})	Symmetry character
	542.8	18 423	A (II)
	541.3	18 473	E
$^5F_4$	540.0	18 518	A (I)
	539.9	18 522	A (II)
	539.6	18 533	E
	539.4	18 539	E (I)
	539.3	18 543	E (II)
$^5F_3$	489.3	20 438	A
	487.6	20 509	A
	487.1	20 530	E
	485.9	20 580	E
	485.4	20 600	A
$^5F_2$	476.8	20 973	E
	475.7	21 022	A
	475.1	21 048	E
$^3K_8$	470.3	21 263	A
	470.2	21 270	E
	469.8	21 287	A
	468.5	21 346	A
	467.8	21 379	A
	467.3	21 398	E
	466.6	21 434	A
$^5G_6$	456.9	21 887	E (I)
	456.6	21 902	E (II)
	455.2	21 970	E
	454.3	22 010	A
	454.0	22 023	A
	453.8	22 034	A
	453.3	22 062	E
	452.2	22 114	A
	451.9	22 129	A (I)
	451.7	22 139	A (II)
	450.7	22 190	E
$^5G_5$	420.5	23 782	E
	420.3	23 793	A (I)
	420.2	23 798	A (II)
	419.1	23 860	A (I)
	418.9	23 872	A (II)
	418.5	23 893	E
	418.0	23 925	E
	417.7	23 942	A
$^5G_4$	390.0	25 642	E
	389.4	25 680	A
	389.0	25 708	E
	388.7	25 730	A
	387.9	25 783	A
$^3K_7$	383.4	26 082	E
	383.2	26 099	A
	382.8	26 127	A

Table 3. Continued.

$^{2S+1}L_J$	Wavelength λ (nm)	Wavenumber E (cm^{-1})	Symmetry character
	382.6	26 138	E
	382.1	26 173	A
$^5G_4$	365.7	27 345	A
	364.6	27 427	A
	363.7	27 498	E
	362.5	27 590	A
	361.9	27 631	E (I)
	361.7	27 648	E (II)
	361.4	27 669	E
	360.8	27 716	A
	360.3	27 756	E
$^3H_6$	349.5	28 610	A
	348.8	28 671	E
	347.8	28 752	A
	346.8	28 835	E
	346.3	28 880	E
	345.0	28 983	A (I)
	344.8	29 003	A (II)
	344.5	29 024	E (I)
	344.3	29 046	E (II)

(I), (II) and ∗ indicate a doublet structure of a single Stark level.

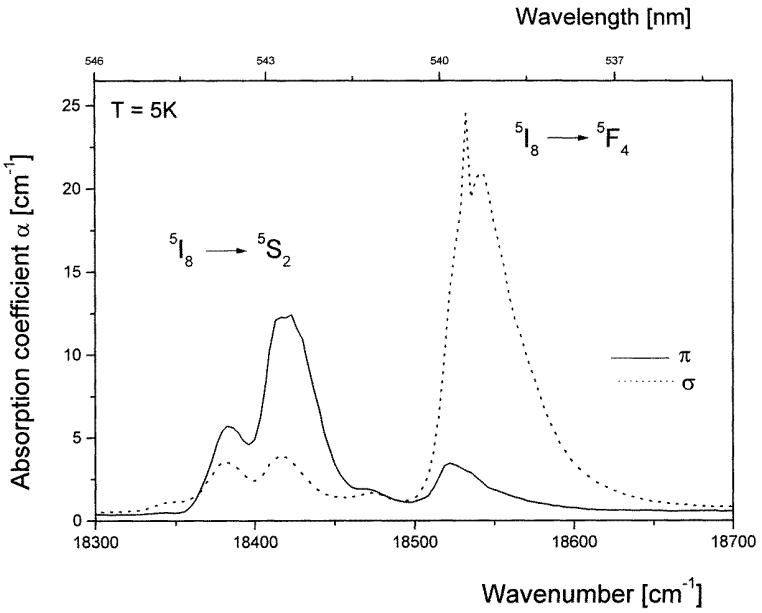

Figure 3. The absorption spectra of the $^5I_8 \rightarrow (^5S_2, {}^5F_4)$ transition of Ho^{3+} in an $LiTaO_3$ crystal at 5 K.

These results clearly indicate that the Ho^{3+} ions occupy more than two (probably four) inequivalent positions in the crystal lattice of $LiTaO_3$ giving splits of order 5, 16,

20 and 34 cm^{-1}. Li^+, Ta^{5+}/Nb^{5+} and the intrinsic vacancy are the natural sites, having trigonal symmetry in $LiTaO_3/LiNbO_3$ crystals. Although Li^+ and Ta^{5+}/Nb^{5+} sites appear as reasonable candidates for metal ion (Ln^{3+}, TM^{3+}) location [7, 18], the replacement of Nb^{5+} antisites and Nb^{5+} vacancies has been identified [13, 19]. Recent investigations show that Ho^{3+} ions in the $LiNbO_3$ host substitute mainly Li^+ sites and only a fraction of the ions occupy other unidentified lattice centres [15]. It is clear that absorption spectra cannot provide direct information on the lattice location of impurities and other techniques are needed.

3.1.2. Radiative transitions—the Judd–Ofelt calculation. Radiative transition rates from the excited states of Ho^{3+} ions in the $LiTaO_3$ crystal have been calculated in the framework of the Judd–Ofelt theory [20, 21]. It should be noted that $LiTaO_3$ is a uniaxial crystal (trigonal symmetry) and the absorption intensities of Ho^{3+} ions will depend on the polarization of the incident light. Therefore, the experimental data obtained from α spectra and from π and σ polarized spectra were used in our calculations. For the area under these spectra the experimental oscillator strengths P_{exp} of the absorption transitions were evaluated using the equation

$$P_p = \frac{mc}{\pi e^2 N} \int \sigma_p(\nu)\,\mathrm{d}\nu \tag{1}$$

where p relates to α, π and σ spectra, m and e are the mass and charge of the electron, c is the velocity of light, N is the number of Ho^{3+} ions per cubic centimetre and $\sigma(\nu)\,\mathrm{d}\nu$ is the integrated absorption coefficient. All transitions were assumed to be electric dipole in nature, except for the $^5I_8 \rightarrow {}^5I_7$ transition which has a magnetic dipole component. In several instances where levels of different J manifolds overlap, the unresolved intensity was assigned to the group of levels. The average energies of the transitions were taken to be the centres of gravity of the absorption bands. For a uniaxial crystal the magnitude of the measured oscillator strengths P_{exp} can be expressed as

$$P_{exp} = \tfrac{1}{3}P_\alpha + \tfrac{1}{3}P_\pi + \tfrac{1}{3}P_\sigma. \tag{2}$$

The obtained values are presented in table 4.

Table 4. Measured and calculated oscillator strengths for Ho^{3+} in $LiTaO_3$.

Transition (from $^5I_8$)	Energy ν (cm^{-1})	Oscillator strength $P \times 10^6$		Residuals $\Delta P \times 10^6$
		Measured	Calculated	
$^5I_7$	5 187	5.38	5.56	0.18
$^5I_6$	8 635	3.71	4.23	0.52
$^5I_5$	11 149	0.75	0.77	0.02
$^5F_5$	15 370	11.47	11.56	0.09
$^5S_2$, $^5F_4$	18 384	15.47	14.88	0.59
$^5F_3$, ($^4F_2$, $^3K_8$), $^5G_6$	21 550	90.0	89.93	0.07
$^5G_5$	23 800	11.22	11.39	0.17
$^5G_4$, $^3K_7$	25 840	2.93	2.40	0.53
$^5G_5$, $^3H_6$	27 455	19.88	20.39	0.51

On the other hand, in the Judd–Ofelt theory, the electric-dipole oscillator strength of a transition from a level J to the level J' is

$$P(a,\ J;\ b,\ J') = \frac{8\pi^2 mc}{3he^2\lambda(2J+1)}\frac{(n^2+2)^2}{9n}S_{ED}(a,\ J;\ b,\ J') \tag{3}$$

where n is the refractive index of the medium ($n = 2.175$ for $LiTaO_3$), and S_{ED} is the electric dipole line strength,

$$S_{ED}(a,\ J;\ b,\ J') = e^2\sum_{t=2,4,6}\Omega_t\left(\langle \mathrm{f}^N J\|U^{(t)}\|\mathrm{f}^N J'\rangle\right)^2. \tag{4}$$

In equation (4) the Ω_t are the phenomenological parameters to be determined for the particular ion–host combination and the squared terms are the matrix elements of the doubly reduced unit tensor $U^{(t)}$ for the rare earth ion whose intermediate coupled eigenstate is represented by $|\mathrm{f}^N J\rangle$. Since the matrix elements are almost host invariant [22] we used values given for Ho^{3+} ions in ZnBS glass [23]. By substituting equation (4) into equation (3) and using the experimentally determined values of the oscillator strengths of the nine observed transitions (table 4) a least-squares-fitting approach was used to find the Ω_t parameters, and the obtained values are $\Omega_2 = 12.6\times10^{-20}$ cm^2, $\Omega_4 = 6.1\times10^{-20}$ cm^2 and $\Omega_6 = 4.3\times10^{-20}$ cm^2. The calculated oscillator strengths are presented in table 4. The contribution of a magnetic dipole transition to the $^5I_8 \rightarrow {}^5I_7$ absorption band has been calculated employing a standard formula and reported matrix elements [24] and subtracting the obtained value from the experimental oscillator strength prior to the fitting procedure.

A measure of the quality of the fit can be noted from the RMS deviation between the measured and calculated oscillator strengths, determined by the relation

$$\mathrm{RMS}\,\Delta P = \left(\frac{\sum(\Delta P)^2}{X-Y}\right)^{1/2} \tag{5}$$

where X is the number of analysed groups of lines ($X = 9$) and Y is the number of fitted parameters ($Y = 3$). In our study RMS ΔP is 4.4×10^{-7}, a value comparable to the RMS ΔP found by applying the Judd–Ofelt theory to other hosts [16, 25].

Having the phenomenological Ω_t parameters one can calculate the radiative transition rates A_r for excited levels according to the formula

$$A_r = \frac{64\pi^4 e^2}{3h(2J+1)\chi^3}\frac{n(n^2+2)^2}{9}\sum_{t=2,4,6}\Omega_t\left|\langle \mathrm{f}^N[L,\ S]J\|U^{(t)}\|\mathrm{f}^N[L',\ S']J'\rangle\right|^2. \tag{6}$$

The calculated values of the radiative transition rates for excited states of Ho^{3+} ions in the $LiTaO_3$ crystal are given in table 5. From these values it is possible to calculate the radiative lifetime of an excited state i:

$$\frac{1}{\tau_r} = \sum_j A_r(i,\ j) \tag{7}$$

and the branching ratio

$$\beta = \frac{A_r(i,\ j)}{\sum_j A_r(i,\ j)} = \tau_r A_r(i,\ j) \tag{8}$$

where the summation is over electric and magnetic dipole transitions to all terminal states j. The values of radiative lifetimes and branching ratios are listed in table 5.

Table 5. Calculated radiative transition rates A_r, luminescence branching ratios β and corresponding radiative lifetimes τ_r for selected excited states of Ho^{3+} in $LiTaO_3$.

$^{S}L_J$	$^{S'}L'_{J'}$	Average wavelength (μm)	A_r (s^{-1})	β	τ_r (μs)
$^5I_7$	$^5I_8$	1.94	566	1.00	1766
$^5I_6$	$^5I_7$	2.75	79	0.05	
	$^5I_8$	4.64	1 400	0.95	676
$^5I_5$	$^5I_6$	4.04	45	0.03	
	$^5I_7$	1.64	879	0.62	709.1
	$^5I_8$	0.89	486	0.35	
$^5F_5$	$^5I_5$	2.40	51	0.00	
	$^5I_6$	1.51	651	0.04	
	$^5I_7$	0.97	3 290	0.19	56.9
	$^5I_8$	0.65	13 573	0.77	
$^5S_2$	$^5F_5$	3.23	5	0.00	
	$^5I_5$	1.39	263	0.01	
	$^5I_6$	1.03	1 116	0.06	
	$^5I_7$	0.75	6 898	0.40	
	$^5I_8$	0.54	9 145	0.53	57.4
$^5F_4$	$^5F_5$	3.30	78	0.00	
	$^5I_5$	1.39	945	0.03	
	$^5I_6$	1.03	1 885	0.06	32.0
	$^5I_7$	0.52	2 819	0.09	
	$^5I_8$	0.54	25 523	0.82	

3.2. Fluorescence data

3.2.1. Fluorescence spectra and lifetimes. The fluorescence spectra have been recorded for unpolarized light at 5 K. The excitation was at 460 nm. The spectra are shown in figures 4 and 5. The bands centred at 18 100 cm^{-1} (550 nm), 15 000 cm^{-1} (660 nm) and 13 200 cm^{-1} (760 nm) were assigned to the transitions $^5S_2 \rightarrow {}^5I_8$, $^5F_5 \rightarrow {}^5I_8$ and $^5S_2 \rightarrow {}^5I_7$, respectively. A weak band at 16 500 cm^{-1} (606 nm) was interpreted as emission from the $^3K_8$ multiplet to the $^5I_7$ state. All of the observed emission bands do not seem fully resolved and show a multi-site structure similar to that observed in absorption.

The lifetime measurements of the emitting levels have been made under excitation with 460 nm ($^5G_6$ multiplet) in the 5–300 K temperature range. The temperature dependence of the fluorescence lifetime in the $^5S_2$ level and $^5F_5$ state is plotted in figure 6. For the low temperature range ($T < 50$ K) we observe a slight increase of measured lifetimes both for the $^5S_2$ state and for the $^5F_5$ level due to the population of the emitting levels by radiative transitions from the upper lying states. Out of this range ($T > 50$ K) with increasing temperature the lifetimes decrease and the character of the curves is a single exponential. With increasing temperature the measured lifetime changes from 19.0 to 13.1 μs for the $^5S_2$ state and from 20.5 to 14.0 μs for the $^5F_5$ level. The radiative lifetimes of the $^5S_2$ and the $^5F_5$ levels are very similar and their values amount to 57.4 and 56.9 μs, respectively.

The differences between the radiative and the fluorescence lifetimes, and the temperature dependence of lifetimes indicates the participation of nonradiative processes in the excited state relaxation such as multiphonon emission and nonradiative energy transfer. The emissions from the $^5S_2$ and $^5F_5$ levels are associated with energy gaps of about 3000 cm^{-1}

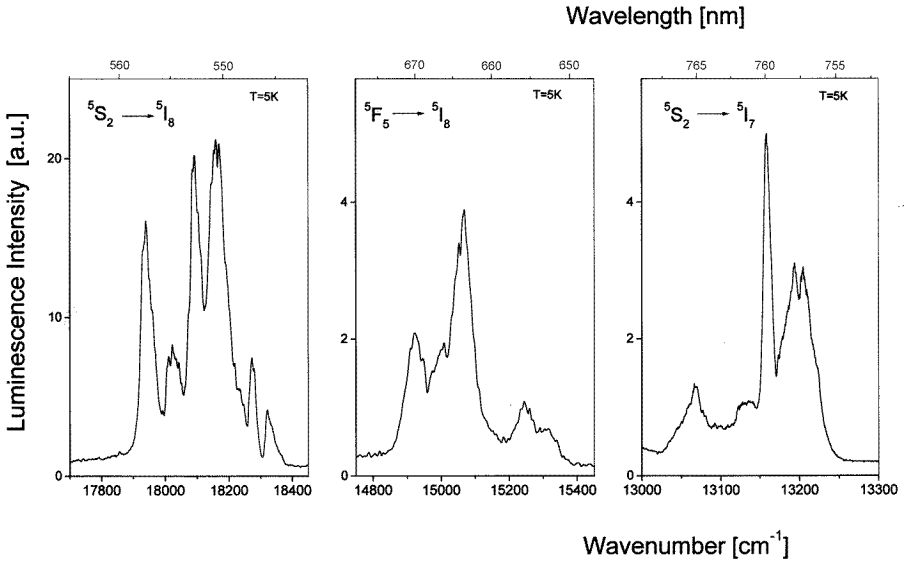

Figure 4. Luminescence spectra of Ho^{3+} in $LiTaO_3$ recorded at 5 K.

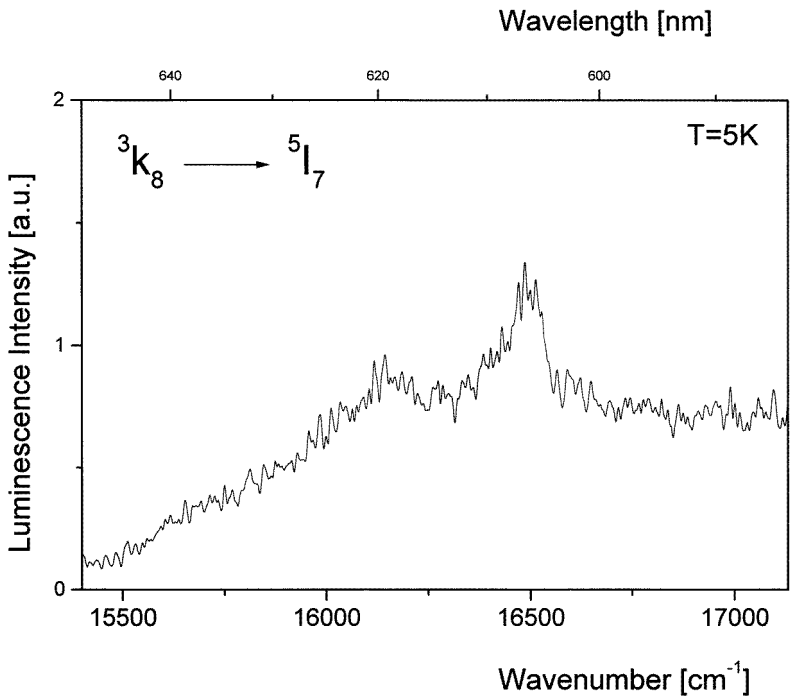

Figure 5. The $^3K_8 \rightarrow {}^5I_7$ emission spectrum of Ho^{3+} in an $LiTaO_3$ crystal measured at 5 K.

($^5S_2 \rightarrow {}^5F_5$) and 2000 cm^{-1} ($^5F_5 \rightarrow {}^5F_4$). The energy of the effective phonon $h\omega_{eff}$ is 598 cm^{-1} in $LiTaO_3$ [26], hence five and three phonons, respectively, are needed to cover the above energy gaps. The nonradiative energy transfer processes can occur between two

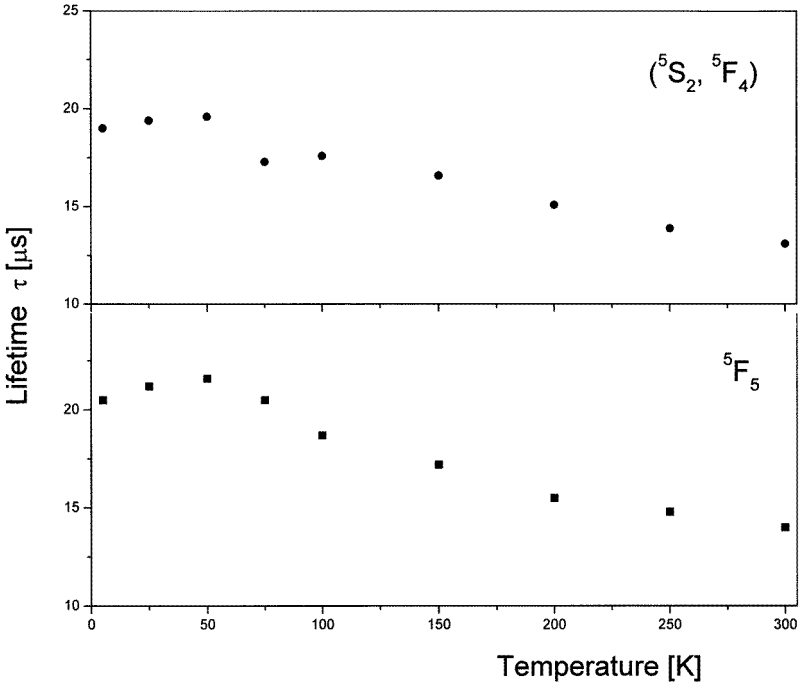

Figure 6. Temperature dependence of the ($^5S_2$, $^5F_4$) and the $^5F_5$ luminescence lifetimes.

near Ho^{3+} ions in different crystalline environments and having some mismatch in their energy levels. A detailed study of ion–ion interactions is needed.

3.3. The $^5I_7 \rightarrow {}^5I_8$ transition—stimulated emission cross-section

The $^5I_7 \rightarrow {}^5I_8$ transition, which is at about 2 μm wavelength, is expected to be the most promising laser action for the Ho^{3+} ion in the $LiTaO_3$ matrix due to its potential application in telecommunication and medicine. The experimental attempt to observe emission from the $^5I_7$ level has failed because of the low power of the excitation source and poor detection system sensitivity, therefore we undertook a theoretical attempt to estimate the emission cross-section curve and to calculate the expected laser gain for this transition.

Emission cross-section is defined as the laser gain per unit population inversion. There are a few ways which lead to numerical calculations of emission cross-section in rare earth laser materials. One of the most popular methods is the so-called reciprocity method. The formula was first derived by McCumber [27] and further developed by Payne *et al* [28] and can be presented as:

$$\sigma_{em}(\lambda) = \sigma_{abs}(\lambda)\frac{Z_l}{Z_u}\exp\left[\left(E_{ul} - \frac{hc}{\lambda}\right)\Big/ kT\right] \tag{9}$$

where $\sigma_{abs}(\lambda)$ is the absorption cross-section defined as $\sigma_{abs} = \alpha/N$, α is the absorption coefficient calculated from the room temperature spectrum, N is the dopant concentration, E_{ul} is the zero-line energy for interacting manifolds and Z_l and Z_u are the partition functions of the lower and upper manifolds, respectively.

The potential laser gain can be calculated as an effective cross-section σ_{eff} from the

emission cross-section obtained by the reciprocity method:

$$\sigma_{eff} = P\sigma_{em} - (1 - P)\sigma_{abs} \tag{10}$$

where P is defined as the ratio of the number of active ions in the excited state to total number of active ions. For all further calculations P values were arbitrary chosen as 0.3, 0.25 and 0.2.

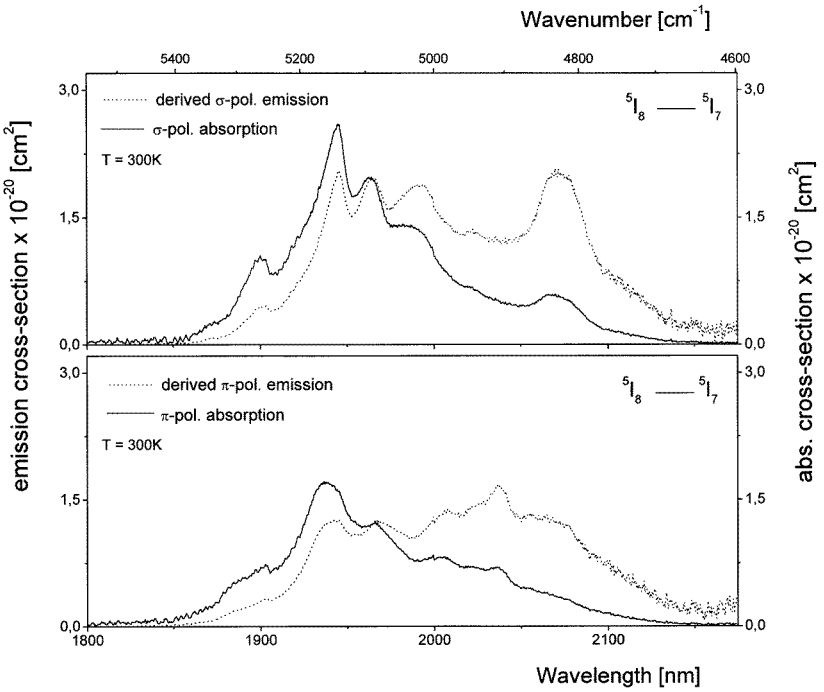

Figure 7. The σ and π polarized absorption cross-section associated with the $^5I_8 \rightarrow {}^5I_7$ transition of Ho^{3+} in $LiTaO_3$ (solid lines) and derived stimulated emission cross-sections (dotted lines) versus wavelength.

The results are presented in figures 7 and 8. In figure 7 we present the σ and π polarized absorption cross-section associated with the $^5I_8 \rightarrow {}^5I_7$ transition (solid lines) and the derived polarized emission cross-section (dashed lines) versus wavelength. The highest value of the emission cross-section is equal to 2.0×10^{-20} cm^2 and was found in the σ spectrum. Figure 8 shows the effective cross-section σ_{eff} curves for both σ and π polarization and for several P values. The presented curves indicate positive laser gain in the 2040–2140 nm wavelength region. A maximum effective cross-section σ_{eff} was found at $\lambda = 2078$ nm in the σ polarized spectrum and its value was estimated as $\sigma_{eff} \approx 0.24 \times 10^{-20}$ cm^2. For comparison, in Ho:Tm:YAG [29] and Ho:Tm:YLF [30] systems, where the energy transfer processes from Tm^{3+} to Ho^{3+} ions are active, the stimulated cross-section, estimated for laser wavelength of about 2 μm, was found to be 1.5×10^{-19} and 0.9×10^{-20} cm^2, respectively.

The analysis of the laser gain allows us to suppose that in the Ho^{3+}:$LiTaO_3$ system the laser oscillation could be achieved within a relatively wide wavelength range.

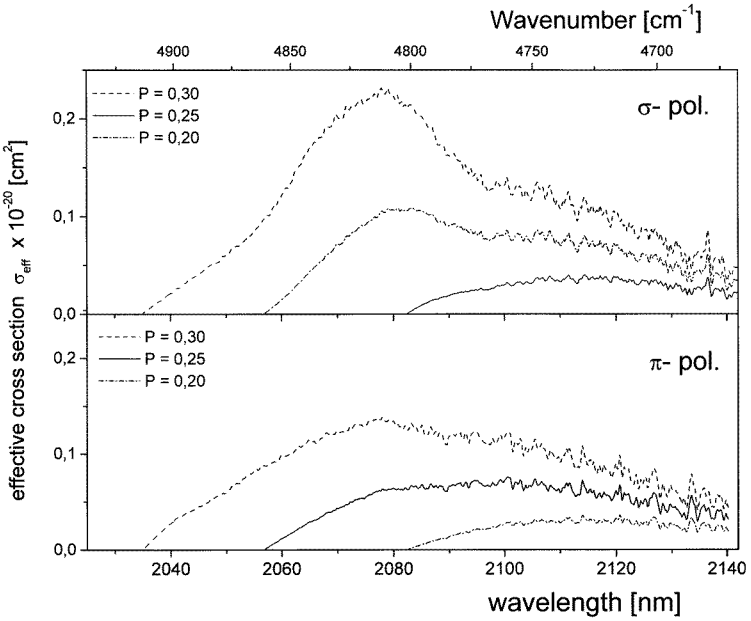

Figure 8. Calculated effective cross-section curves versus wavelength for different P values.

4. Conclusion

The present study yields a detailed picture of the spectroscopic characteristics of the Ho^{3+} ions in the $LiTaO_3$ crystal. The optical study has been carried out in the visible and near infrared range of the spectrum in the 5–300 K temperature range. The energy level data and analysis reported here provide a good description of the $4f^{10}$ energy level structure. Using the selection rules for C_3 symmetry for polarized absorption data analysis gives information on the Stark level multiplets and polarized character of the observed transitions. The coexistence of the different lattice sites for Ho^{3+} ions has been detected both in absorption spectra and in emission.

The Judd–Ofelt formalism was used to calculate the radiative transition rates, radiative lifetimes and branching ratios of the excited states of the Ho^{3+}-doped $LiTaO_3$ crystal. The comparison with the fluorescence data thus shows that the nonradiative relaxation is important. The differences between the measured and the radiative lifetimes are due to multiphonon emission and energy transfer.

Finally, the emission cross-section around 2000 nm was determined from the room temperature absorption spectrum due to the $^5I_8 \rightarrow {}^5I_7$ transition and the stimulated emission probabilities. A maximum value of emission cross-section σ_{em} of about 2×10^{-20} cm^2 was found for the derived σ polarized emission spectrum at 2.08 μm.

References

[1] Garcia Solé J, Lou L, Monteil A, Boulon G, Lecocq S, Vergara I, Camarillo E and Cochet-Muchy D 1993 *Eur. J. Solid State Inorg. Chem.* **30** 1049

[2] Abedin K S, Sato M and Ito H 1995 *J. Appl. Phys.* **78** 691

[3] Nouh S, Baldi P, El Hadi K, De Micheli M, Monnom G, Ostrowsky D B, Lallier E and Papuchon M 1995 *Opt. Lett.* **20** 1468
[4] Burlot R, Moncorgé R, Manaa H, Boulon G, Guyot Y, Garcia Solé J and Cochet-Muchy D 1996 *Opt. Mater.* **6** 313
[5] Abedin K S, Tsuritani T, Sato M and Ito H 1997 *Appl. Phys. Lett.* **70** 10
[6] Sokólska I, Ryba-Romanowski W, Gołab S and Łukasiewicz T 1997 *Appl. Phys.* B **65** 495
[7] Sokólska I, Ryba-Romanowski W, Gołab S, Łukasiewicz T and Świrkowicz M 1997 *J. Phys.: Condens. Matter* **9** 5217
[8] Nikl M, Morlotti R, Magro C and Bracco R 1996 *J. Appl. Phys.* **79** 2853
[9] Glass A M 1968 *J. Chem. Phys.* **50** 1501
[10] Ryba-Romanowski W, Gołab S, Pisarski W A and Dominiak-Dzik G 1997 *Appl. Phys. Lett.* **70** 1
[11] Zotov N, Boysen H, Frey F, Metzger T and Born E 1994 *J. Phys. Chem. Solids* **55** 145
[12] Lorenzo A, Jaffrezic H, Roux B, Boulon G and Garcia Solé J 1995 *J. Appl. Phys. Lett.* **67** 3735
[13] Macfarlane P I, Holliday K, Nicholls J F H and Henderson B 1995 *J. Phys.: Condens. Matter* **7** 9643
[14] Henderson B and Imbusch G P 1989 *Optical Spectroscopy of Inorganic Solids* (Oxford: Clarendon)
[15] Lorenzo A, Bausá L E and Garcia Solé J 1994 *J. Phys.: Condens. Matter* **6** 1065
[16] Lorenzo A, Bausá L E, Sanz-Garcia J A and Garcia Solé J 1996 *J. Phys.: Condens. Matter* **8** 5781
[17] Johnson L F and Ballman A A 1969 *J. Appl. Phys.* **40** 297
[18] Vergara I, Camarillo E, Sanz-Garcia J A, Garcia Solé J, Jaque F, Monteil A and Boulon G 1992 *Solid State Commun.* **82** 733
[19] Tocho J O, Camarillo E, Cusso F, Jaque F and Garcia Solé J 1991 *Solid State Commun.* **80** 575
[20] Judd B R 1962 *Phys. Rev.* **127** 750
[21] Ofelt G S 1962 *J. Chem. Phys.* **37** 511
[22] Reisfeld R, Katz G, Jacoboni C, DePape R, Drexhage M G, Brown R N and Jørgensen C K 1983 *J. Solid State Chem.* **48** 323
[23] Rukmini E and Jayasankar C K 1995 *Opt. Mater.* **4** 529
[24] Carnall W T, Fields P R and Rajnak K 1968 *J. Chem. Phys.* **49** 4412
[25] Tanimura K, Shinn M D and Sibley W A 1984 *Phys. Rev.* B **30** 2429
[26] Palatnikov M N, Sandler V A, Serebryakov Yu A, Sidorov N V and Kalinnikov V T 1996 *Ferroelectrics* **175** 183
[27] McCumber D E 1973 *Phys. Rev.* A **136** 758
[28] Payne S A, Chase L L, Newkirk H W, Smith L K and Krupke W F 1988 *IEEE J. Quantum Electron.* **24** 2243
[29] Kubo T S and Kane T J 1992 *IEEE J. Quantum Electron.* **28** 1033
[30] Storm M E 1993 *IEEE J. Quantum Electron.* **29** 440